Supplementary Information: Hydrogen Defects in LaBi$_2$O$_4$X (X=Cl, Br, and I) Sillén Oxyhalide Phases and their Impacts on Ionic Transport

ShinYoung Kang[1], Andrew J. E. Rowberg[1], Shenli Zhang[1,2], Joel B. Varley[1,*]

1. Materials Science Division and Laboratory for Energy Application for the Future (LEAF), Lawrence Livermore National Laboratory, Livermore, California 94550, USA
2. Current affiliation: Department of Chemical and Materials Engineering, San José State University, San Jose, California 95192, USA

* Corresponding Author: Joel B. Varley, varley2@llnl.gov

DFT calculation settings

Defect calculations were performed using the Vienna *Ab initio* Simulation Package (VASP)[1] based on the projector augmented wave (PAW) method [2] with a plane-wave energy cutoff of 400 eV. The Perdew–Burke–Ernzerhof (PBE) generalized gradient approximation (GGA) functional [3] was used to compute the total energies of both pristine and defect-containing supercells. The initial structural parameters for tetragonal LaBi$_2$O$_4$X (X = Cl, Br, or I) were optimized for the primitive unit cells, each containing one formula unit, until the total energy and atomic forces converged to below 10^{-6} eV and 10^{-2} eV/Å, respectively, with a $6 \times 6 \times 2$ Γ-centered k-point mesh. The formation energies of hydrogen-related defects were evaluated using $3 \times 3 \times 2$ supercells using the standard supercell formalism [4]. In these defect calculations, atomic positions were relaxed while the lattice parameters were fixed to those of the relaxed bulk. k-points were sampled using $3 \times 3 \times 2$ Monkhorst−Pack grids. Convergence thresholds for the total energy and forces were set to 10^{-3} eV and 5×10^{-2} eV/Å, respectively. For charged defects, spurious electrostatic interactions between periodic images were corrected using the Freysoldt–Neugebauer–Van de Walle (FNV) scheme [5]. Due to the tetragonal symmetry, the only nonzero components of the dielectric tensor are $\varepsilon_{xx} = \varepsilon_{yy}$ and ε_{zz}; these values are $\varepsilon_{xx} = 34.05$ and $\varepsilon_{zz} = 14.91$ for LaBi$_2$O$_4$Cl, $\varepsilon_{xx} = 32.28$ and $\varepsilon_{zz} = 14.16$ for LaBi$_2$O$_4$Br, and $\varepsilon_{xx} = 31.54$ and $\varepsilon_{zz} = 14.53$ for LaBi$_2$O$_4$I. The defect types and charge states examined in this work are summarized in Table S1. Migration barriers of selected defects were determined using the Climbing Image Nudged Elastic Band (CI-NEB) method [6]. Depending on the hopping distance, 1, 3, or 5 intermediate images were used.

Additional calculations using the screened hybrid functional of Heyd-Scuseria-Ernzerhof (HSE06) [7] with a mixing parameter of 25% and a screening parameter of 0.2 Å^{-1} were used, in conjunction with spin–orbit coupling (SOC) to evaluate the band gap (E_g) and band edge shifts relative to those obtained with PBE. These parameters have been shown to yield band gaps and lattice parameters in good agreement with experiment [8-11], with values summarized in Table S2. The electronic densities of states computed with this approach are illustrated in Figs S1-2. Single-point HSE06+SOC calculations were performed using the GGA-optimized lattice parameters, and the resulting valence band maximum (VBM) and band gap values were used to compute the defect formation energies (see Eq. S1 in the next section).

Table S1. List of point defects considered in this study. We attempted to construct $[H_i - V_O]$ and $[OH_i - V_O]$ complexes, but the relaxed structures see the interstitial species spontaneously relax to the vacant oxygen site, forming H_O and $[H_i - O_O]$, respectively.

Defect	Charge state	Defect	Charge state	Defect	Charge state
H_i	-1, +1	H_O	0, +1	V_X	-1, 0, +1
O_i, $O_i(db)$	-2, 0	OH_i	-1	H_X	-1, 0, +1, +2
V_O	+2	$[H_i - V_X]$	-1, 0, +1	$[O_i - V_O]$	0

Table S2. Summary of lattice constants and band gaps in tetragonal LaBi$_2$O$_4$X (X=Cl, Br, I).

X	Lattice constant from PBE		Lattice constant from HSE		Band gap in eV			
	a = b (Å)	c (Å)	a = b (Å)	c (Å)	PBE	HSE @ PBE cell	HSE	Experiment
Cl	3.944	8.892	3.915	8.949	1.21	2.01	2.04	2.65[9], 2.79[10]
Br	3.963	9.061	3.940	9.174	1.08	1.80	1.84	N/A
I	3.994	9.267	3.972	9.479	1.21	1.72	1.75	N/A
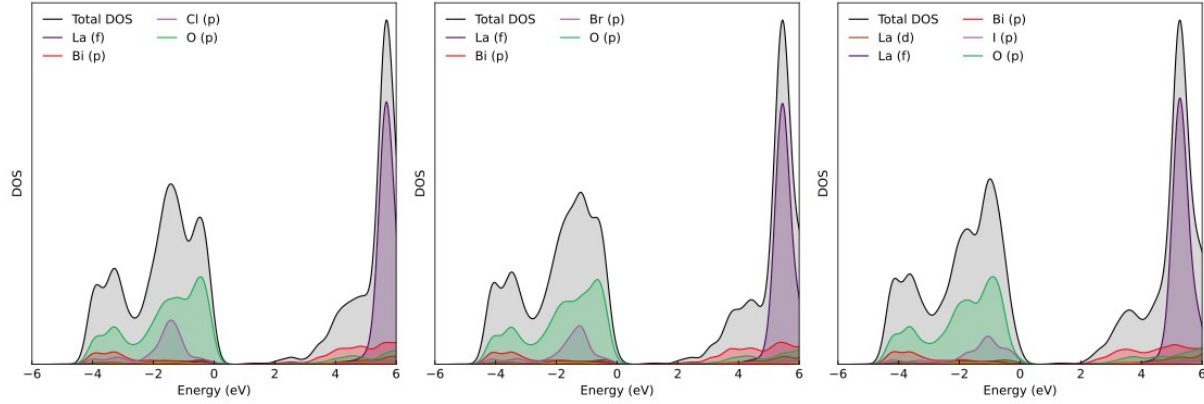
Figure S 1. Electronic density of states in (a) $LaBi_2O_4Cl$, (b) $LaBi_2O_4Br$, and (c) $LaBi_2O_4I$ calculated in the PBE functional. The Fermi level is set to zero. The energy bandgaps are 1.21, 1.08, and 1.21 eV, respectively.
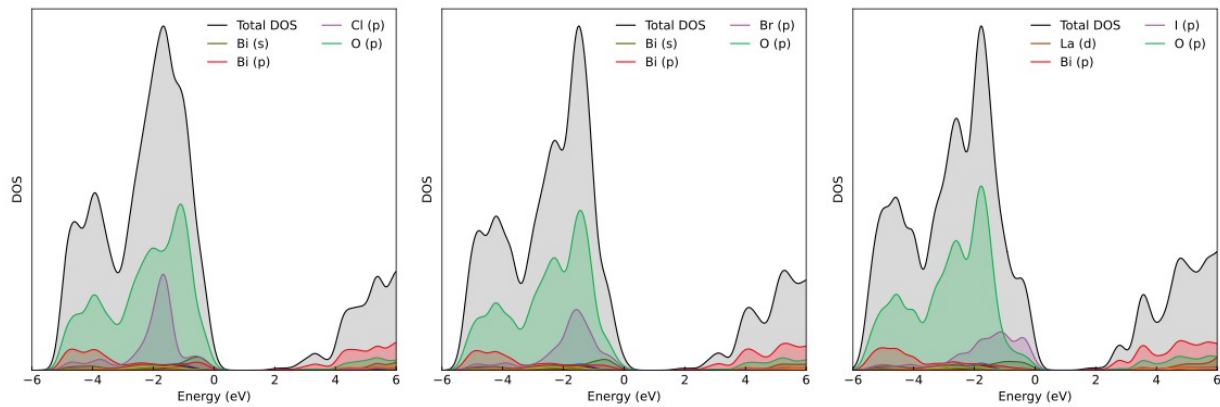

Figure S 2. Electronic density of states in (a) $LaBi_2O_4Cl$, (b) $LaBi_2O_4Br$, and (c) $LaBi_2O_4I$ calculated in the HSE06 functional with the spin-orbit coupling considered. The Fermi level is set to zero. The lattice constants were fixed to those relaxed in the PBE functional. The energy bandgaps are 2.01, 1.80, and 1.72 eV, respectively.

Defect formation energy

The formation energy of defect X in charge state q is given by:

$$E^{\text{f}}[X^q] = E_{\text{tot}}[X^q] - E_{\text{tot}}[\text{bulk}] - \sum_i n_i \mu_i + q(E_{VBM} + E_F) + E_{\text{corr}}, \qquad \text{eq. S1}$$

where $E_{\text{tot}}[X^q]$ and $E_{\text{tot}}[\text{bulk}]$ are the total energies of the defective and pristine supercells, respectively. n_i is the number of atoms of species i added to (n_i negative) or removed from (n_i positive) the supercell, μ_i is the corresponding chemical potential, E_{VBM} denotes the valence band maximum of the pristine bulk, E_F is the Fermi level referenced to the VBM, and E_{corr} is the correction energy from the FNV scheme.

Defect binding energies were calculated by subtracting the formation energies of reactant defects (A and B), from that of the product defect complex (C), $BE[C] = E^{\text{f}}[C] - E^{\text{f}}[A] - E^{\text{f}}[B]$.

All quantities except for the band-edge positions were computed using the PBE functional. The VBM and conduction band minimum (CBM) levels were subsequently adjusted to match those obtained from the HSE06 + SOC calculations. Figure S3 schematically illustrates the relative positions of the VBM and CBM from both functionals and their effect on defect formation energies and charge-transition levels. The HSE06 hybrid functional lowers the VBM and slightly raises the CBM, thereby widening the band gap. This shift manly stabilizes positively charged defects (e.g., H_i^+) and destabilizes negatively charged ones (e.g., O_i^{2-}).
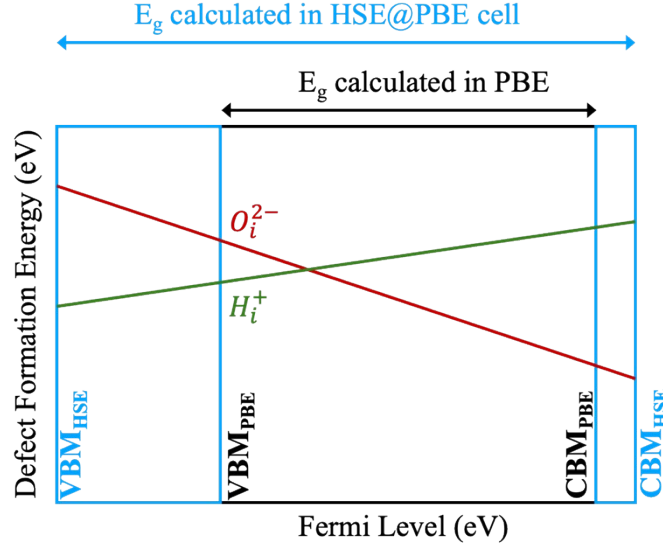
Figure S 3. Illustration of adjustments of band edges and defect formation energies from the GGA PBE to HSE06. The HSE06 calculations were performed using the pristine bulk which lattice constants are fixed to those optimized in the PBE functional.

Chemical potential references

The chemical potential of element A, $\Delta\mu_A$, is expressed as a deviation from the ground state energy:

$$\mu_A = \Delta\mu_A + E(A),$$ eq. S2

where $E(A)$ is the elemental reference energies were obtained within DFT-PBE: isolated O_2, H_2, Cl_2, Br_2, and I_2 molecules for the gaseous elements; La metal in the hexagonal close-packed ($P6_3/mmc$) structure; and Bi metal in the rhombohedral ($R\overline{3}m$) structure. Their total energies in the PBE functional are denoted as $E_{DFT}^{tot}(X)$.

We considered the oxygen-rich limit where the oxygen chemical potential was set as $\Delta\mu_O = 0$ eV/O, corresponding to $\mu_O = \frac{1}{2} E_{DFTtot}(O_2) = -4.939$ eV/O. Next, the hydrogen chemical potential was set under equilibrium with water formation: $H_2 + \frac{1}{2}O_2 \rightarrow H_2O$, with the reaction enthalpy $\Delta H_{form}^{expt}(H_2O) = 2.960$ eV per H_2O at the standard state. This yields $\Delta\mu_H = \frac{1}{2}\Delta H_{form}^{expt}(H_2O) - \frac{1}{2}\Delta\mu_O = -1.480$ eV/H, corresponding to $\mu_H = \frac{1}{2} E_{DFTtot}(H_2) + \Delta\mu_H = -4.860$ eV/H.

For the chemical potentials of La, Bi, and halogen element X, first, we assumed conditions ensuring the thermodynamic stability of the Sillén phases:

$$\Delta H_{\text{form}}(LaBi_2O_4X) \cong \Delta E_{\text{form}}(LaBi_2O_4X) = \Delta\mu_{La} + 2\Delta\mu_{Bi} + 4\Delta\mu_O + \Delta\mu_X, \qquad \text{eq. S3}$$

where $\Delta H_{\text{form}}(LaBi_2O_4X)$ is the enthalpy of formation of the $LaBi_2O_4X$ Sillén phases, and $\Delta E_{\text{form}}(LaBi_2O_4X)$ is the approximated form of ΔH_{form} computed using the total energies from DFT-PBE calculations. Based on the Li-Bi-O-X phase diagrams from the Materials Project [12], we placed additional limits on the chemical potentials to prevent the precipitation of competing phases:

$$\Delta H_{\text{form}}(La_2O_3) \cong \Delta E_{\text{form}}(La_2O_3) \geq 2\Delta\mu_{La} + 3\Delta\mu_O, \qquad \text{eq. S4}$$

$$\Delta H_{\text{form}}(Bi_2O_3) \cong \Delta E_{\text{form}}(Bi_2O_3) \geq 2\Delta\mu_{Bi} + 3\Delta\mu_O, \qquad \text{eq. S5}$$

$$\Delta H_{\text{form}}(BiOX) \cong \Delta E_{\text{form}}(BiOX) \geq \Delta\mu_{Bi} + \Delta\mu_O + \Delta\mu_X, \qquad \text{eq. S6}$$

$$\Delta H_{\text{form}}(LaX_3) \cong \Delta E_{\text{form}}(LaX_3) \geq \Delta\mu_{La} + 3\Delta\mu_X, \text{ and} \qquad \text{eq. S7}$$

$$\Delta H_{\text{form}}(BiX_3) \cong \Delta E_{\text{form}}(BiX_3) \geq \Delta\mu_{Bi} + 3\Delta\mu_X. \qquad \text{eq. S8}$$

The formation energies of the competing phases along with the $LaBi_2O_4X$ Sillén phases are summarized in Table S3. Among the chemical potential sets ensuring the stability of $LaBi_2O_4X$ relative to other compounds, we chose the oxygen- and halogen-rich limits (Table S4) to calculate the defect formation energies in eq. S1.

Table S3. Formation energies of $LaBi_2O_4X$ (X = Cl, Br, I) and their competing compounds.

Compound	ΔE_{form} (eV/f.u.)	Compound	ΔE_{form} (eV/f.u.)	Compound	ΔE_{form} (eV/f.u.)	Compound	ΔE_{form} (eV/f.u.)
$LaBi_2O_4Cl$	-16.08	BiOCl	-3.81	$LaCl_3$	-9.77	$BiCl_3$	-3.84
$LaBi_2O_4Br$	-15.85	BiOBr	-3.55	$LaBr_3$	-8.48	$BiBr_3$	-3.44
$LaBi_2O_4I$	-15.34	BiOI	-3.11	LaI_3	-6.73	BiI_3	-2.46
La_2O_3	-17.26	Bi_2O_3	-6.14				

Table S4. Chemical potentials at oxygen- and halogen-rich conditions ensuring the materials stability of LaBi$_2$O$_4$X (X = Cl, Br, I) phases.

Chemical potential (eV)	LaBi$_2$O$_4$Cl	LaBi$_2$O$_4$Br	LaBi$_2$O$_4$I
$\Delta\mu_{La}$	-8.79	-8.76	-9.11
$\Delta\mu_{Bi}$	-3.48	-3.55	-3.11
$\Delta\mu_{O}$	0.00	0.00	0.00
$\Delta\mu_{X}$	-0.33	0.00	0.00

Band alignment via work function calculations

        Symmetric, off-stoichiometric (001) surface slabs were constructed by extending the unit cell fourfold along the c-axis to obtain the planar-averaged electrostatic potential. The bulk-averaged potential, $\phi_{\text{bulk, PBE}}^{\text{avg}}$, and vacuum level, ϕ_{vacuum}, were calculated using the PBE functional. These quantities defined the alignment of the band edges (VBM$_{\text{PBE}}$ and CBM$_{\text{PBE}}$, as well as VBM$_{\text{HSE}}$ and CBM$_{\text{HSE}}$) relative to ϕ_{vacuum}. Representative results for LaBi$_2$O$_4$Cl are shown in Fig. S4, where the averaged potential is plotted along the c-axis.

        The corresponding absolute energy levels (with respect to the vacuum level) are summarized in Table S5. The oxygen evolution reaction (OER) potential, 1.23 V vs. the standard hydrogen electrode, corresponds to $E = -5.67 \text{ eV}$ with respect to vacuum.
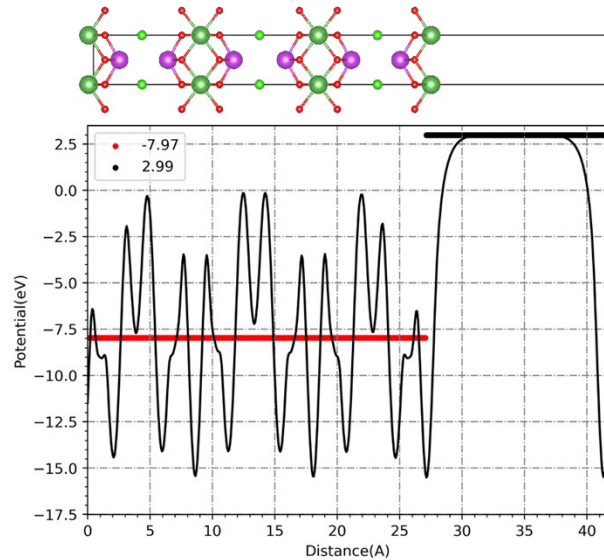

Figure S 4. Example work function calculations in LaBi$_2$O$_4$Cl using the PBE functional. A thin black line is the ionic and Hartree potential averaged over the ab planes as a function of c-axis distance. The structure is illustrated on the top. Red and black lines are the average potential in the material bulk ($\phi_{\text{bulk, PBE}}^{\text{avg}}$) and vacuum ($\phi_{\text{vacuum}}$), respectively.
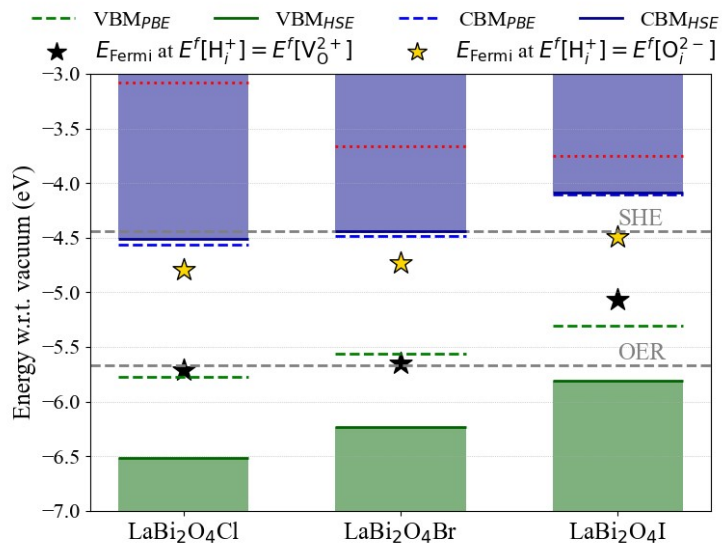
Figure S 5. Energy level diagram identical to Figure 3(a), but with the charge transition level $\varepsilon(V^{2+}_O | V^0_O)$ denoted by red dotted lines. The $\varepsilon(V^{2+}_O | V^0_O)$ levels were computed with the HSE06 functional, and their positions higher than the CBM$_{HSE}$ indicate that oxygen vacancy acts as a double donor across the entire band gaps in all materials.

Table S5. Energy level alignment across -Cl, -Br, and -I Sillén phases using the vacuum level. The oxygen evolution reaction (OER) potential, which is 1.23 V versus the standard hydrogen electrode, corresponds to ϕ_{OER}= -5.67 eV with respect to the vacuum level, ϕ_{vacuum}.

Energy levels and defect formation energies (eV)		X=Cl	X=Br	X=I
With respect to $\phi_{bulk,\ PBE}^{avg}$	VBM$_{PBE}$	5.19	5.21	5.81
	VBM$_{HSE}$	4.44	4.54	5.31
	CBM$_{PBE}$	6.40	6.29	7.02
	CBM$_{HSE}$	6.45	6.33	7.03
With respect to ϕ_{vacuum}	$\phi_{bulk,\ PBE}^{avg}$	-10.96	-10.77	-11.12
	VBM$_{PBE}$ (= -IP$_{PBE}$)	-5.77	-5.56	-5.31
	VBM$_{HSE}$ (= -IP$_{HSE}$)	-6.52	-6.23	-5.81
	CBM$_{PBE}$	-4.56	-4.48	-4.10
	CBM$_{HSE}$	-4.51	-4.44	-4.09
	E_{Fermi} when $E^f\left[H_i^+\right] = E^f\left[V_O^{2+}\right]$	-5.71	-5.65	-5.07
	E_{Fermi} when $E^f\left[H_i^+\right] = E^f\left[O_i^{2-}\right]$	-4.79	-4.73	-4.49
$E^f\left[H_i^+\right]$ when $E_{Fermi} = \phi_{OER}$		-0.05	-0.02	-0.23
$E^f\left[H_i^+\right]$ when $E_{Fermi} = -5\ eV$		0.62	0.65	0.44

Table S6. Relative valence-band maximum energies, ΔVBM_{HSE}, of $LaBi_2O_4X$ (X = Cl, Br, I) with respect to $LaBi_2O_4Cl$. Results obtained using bulk core-level alignment (Bi 1s, La 1s, and O 1s eigenvalues) are compared with those obtained from vacuum-level alignment via the IP_{HSE} values from Table S5. All values are given in eV. For the determination of absolute band positions, vacuum-level alignment provides the appropriate reference, as it directly yields band energies with respect to the vacuum level and includes surface-induced electrostatic potential offsets. Bulk core-level alignment, while useful for assessing intrinsic bulk band-edge trends, does not capture these contributions and therefore underestimates the full shift in absolute band energies.

Alignment method	X=Cl	X=Br	X=I
Vacuum level (ΔIP_{HSE})	0.00	0.29	0.71
Bi 1s core level	0.00	0.22	0.38
La 1s core level	0.00	0.25	0.43
O 1s core level	0.00	0.22	0.39

References

(1) Furthmüller, J.; Kresse, G. Efficient iterative schemes for ab initio total-energy calculations using a plane-wave basis set. *Physical Review B* **1996**, *54*, 11169.

(2) Blöchl, P. E. Projector augmented-wave method. *Physical Review B* **1994**, *50*, 17953.

(3) Perdew, J. P.; Burke, K.; Ernzerhof, M. Generalized gradient approximation made simple. *Physical Review B* **1996**, *77*, 3865. DOI: 10.1103/PhysRevLett.77.3865.

(4) Freysoldt, C.; Grabowski, B.; Hickel, T.; Neugebauer, J.; Kresse, G.; Janotti, A.; Van de Walle, C. G. First-principles calculations for point defects in solids. *Reviews of Modern Physics* **2014**, *86* (1), 253-305. DOI: 10.1103/RevModPhys.86.253.

(5) Freysoldt, C.; Neugebauer, J.; Van de Walle, C. G. Fully Ab Initio Finite-Size Corrections for Charged-Defect Supercell Calculations. *Physical Review Letters* **2009**, *102* (1), 016402. DOI: 10.1103/PhysRevLett.102.016402.

(6) Henkelman, G.; Arnaldsson, A.; Jonsson, H. A fast and robust algorithm for Bader decomposition of charge density. *Computational Materials Science* **2006**, *36* (3), 354-360, Article. DOI: 10.1016/j.commatsci.2005.04.010.

(7) Krukau, A. V.; Vydrov, O. A.; Izmaylov, A. F.; Scuseria, G. E. Influence of the exchange screening parameter on the performance of screened hybrid functionals. *The Journal of Chemical Physics* **2006**, *125* (22). DOI: 10.1063/1.2404663 (acccessed 10/7/2025).

(8) Milne, C. J.; Lightfoot, P.; Jorgensen, J. D.; Short, S. Synthesis and structure of Bi2LaO4Cl: a novel variant of the sillen phases. *Journal of Materials Chemistry* **1995**, *5* (9), 1419-1421, 10.1039/JM9950501419. DOI: 10.1039/JM9950501419.

(9) Meng, J.; Sheikh, M. S.; Schultz, L. E.; Nachlas, W. O.; Liu, J.; Polak, M. P.; Jacobs, R.; Morgan, D. Ultrafast Oxygen Conduction in Sillén Oxychlorides. *Chemistry of Materials* **2025**, *37* (9), 3147-3157. DOI: 10.1021/acs.chemmater.4c03163.

(10) Nakada, A.; Kato, D.; Nelson, R.; Takahira, H.; Yabuuchi, M.; Higashi, M.; Suzuki, H.; Kirsanova, M.; Kakudou, N.; Tassel, C.; et al. Conduction Band Control of Oxyhalides with a Triple-Fluorite Layer for Visible Light Photocatalysis. *Journal of the American Chemical Society* **2021**, *143* (6), 2491-2499. DOI: 10.1021/jacs.0c10288.

(11) Schmidt, M.; Oppermann, H.; Hennig, C.; Henn, R. W.; Gmelin, E.; Söger, N.; Binnewies, M. Untersuchungen zu Bismutseltenerdoxidhalogeniden der Zusammensetzung Bi2SEO4X (X=Cl, Br, I). *Zeitschrift für anorganische und allgemeine Chemie* **2000**, *626* (1), 125-135. DOI: https://doi.org/10.1002/(SICI)1521-3749(200001)626:1<125::AID-ZAAC125>3.0.CO;2-S (acccessed 2025/10/24).

(12) Jain, A.; Ong, S. P.; Hautier, G.; Chen, W.; Richards, W. D.; Dacek, S.; Cholia, S.; Gunter, D.; Skinner, D.; Ceder, G.; et al. Commentary: The Materials Project: A materials genome approach to accelerating materials innovation. *APL Materials* **2013**, *1* (1), 011002. DOI: 10.1063/1.4812323 (acccessed 2/4/2025).